BNL-108453-2015-JA

Structurally Ordered Pt-Zn/C Series Nanoparticles as Efficient Anode Catalysts for Formic Acid Electrooxidation

Jing Zhu,[a] Xin Zheng,[a] Jie Wang,[a] Zexing Wu,[a] Lili Han,[b] Ruoqian Lin,[b] Huolin L. Xin,[b,c] and Deli Wang*[a]

Controlling the size, composition, and structure of bimetallic nanoparticles is of particular interest to electrocatalysts for fuel cells. In the present work, structurally ordered nanoparticles with intermetallic phases of Pt_3Zn and PtZn have been successfully synthesized via an impregnation reduction method, followed by post heat-treatment. The Pt_3Zn and PtZn ordered intermetallic nanoparticles are well dispersed on the carbon support with ultrasmall mean particle sizes of ~5 nm and ~3 nm in diameter, respectively, which are credited to the evaporation of zinc element at high temperature. Meanwhile these catalysts are less susceptible to CO poisoning relative to Pt/C and exhibited enhanced catalytic activity and stability toward formic acid electrooxidation. The mass activities of as-prepared catalysts were approximately 2 to 3 times that of commercial Pt at 0.5 V (vs. RHE). The facile synthetic strategy is scalable for mass producing catalytic materials.

Introduction

Direct formic acid fuel cells (DFAFCs) have attracted increasing interest over the past decade as a power source for portable electronic devices because of the two major advantages of formic acid (HCOOH) as liquid fuel, namely much lower crossover flux through Nafion membrane[1-3] than that of methanol, and a higher theoretical open circuit potential (1.48 V) than that of hydrogen fuel cells (1.23 V) and direct methanol fuel cells (1.21 V).[4, 5] In addition, the merits of HCOOH possess less toxicity than methanol, and allowing the use of highly concentrated fuel.[6] However, the electro-oxidation of HCOOH remains challenging because conventional catalysts such as platinum (Pt) are susceptible to poisoning by carbon monoxide (CO), a reaction intermediate in the HCOOH catalytic process.[7-9] This poisoning, adsorbed CO can only be oxidized up to excessive potential at +0.75 V,[10] which seriously reduces the catalytic performance of Pt electrode. Therefore, multi-metallic catalysts such as Pt-M (M: Bi,[11-14] Pd,[15-18] Au,[19-21] Zn,[22-25] et al.) are required for their geometric and electronic effects, altering the electronic properties of Pt, in a way that enhances resistance to CO poisoning including impeding the CO production and facilitating the oxidation of adsorbed CO at relatively lower potentials.[26] Moreover, it has been reported that intermetallic PtZn[22] and Pt_3Zn[23] nanoparticles exhibited high activities toward formic acid and methanol oxidation. However, the comparison of catalytic activity and stability of intermetallic Pt-Zn series nanoparticles via an improved impregnation reduction method, followed by post heat-treatment has not been reported.

Recently, structurally ordered Pt-based intermetallic nanocatalysts have been studied beyond the disordered alloys because the electronic and geometric structure of ordered intermetallic nanocatalysts can be precisely tuned.[27-30] Moreover, the dissolution of the alloyed elements in an ordered structure could be reduced under harsh operation condition of fuel cells.[31] Nevertheless, to date, chemically ordered structure is rarely considered as a factor to affect the catalytic activities. It is very likely that the intermetallic phase is hard obtained without sacrificing other parameters of nanoparticles, such as size, shape, and composition.[32-34] For example, particle aggregation/sintering[35] and morphology changing[23] are usually found under high temperature annealing conditions that is generally necessary to obtain ordered phases. It is well known that the performance of a catalyst layer in a fuel cell is influenced by particle size,[36-38] generally, the smaller particle size, the higher the surface area to volume ratio and more active sites. Herein, structurally ordered Pt-Zn/C series nanoparticles with mean particle sizes of 3 to 5 nm have been successfully prepared by using a simple impregnation reduction method, followed by a post temperature treatment. Owing to an enormous difference of surface energy between platinum and zinc, some of zinc atoms segregated to the surface during thermal annealing, preventing the sintering of Pt nanoparticles while forming an ordered phase.

For the wet chemical synthesis of Pt-*3d* transition metal nanoparticles, an ultrafast and powerful reducing process is needed to reduce transition metals' precursors and incorporate them into platinum lattice,[39] which means using a very strong reducing agent. In the case of Pt-Zn system, it is very difficult to achieve because the standard reduction potential of Zn^{2+}/Zn is as low as -0.76 V.[25] It often relied on the use of organic surfactant molecules to stabilize particles against agglomeration. However, the surfactant

could not be easily removed and often decomposed into a carbonaceous coating, rendering the particles inactive toward formic acid oxidation during annealing to obtain the intermetallic phase.[40] In this study, carbon supported Pt and Zn precursors were reduced in a tube furnace with flowing H_2, clean alloy nanoparticles were obtain successfully at 300 ºC. Interestingly, according to thermodynamic calculation, Zn^{2+} cannot be reduced by H_2 at 300 ºC, due to the positive free Gibbs energy. It can be explained by hydrogen spillover phenomenon, in which the high active hydrogen atoms, not hydrogen molecules, may spillover from Pt, to reduce adjacent chemisorbed Zn^{2+} to their elemental state.[41] Thus, when the nominal ratio of Pt to Zn is up to 3:10, Zn^{2+} could not be reduced completely, owing to limited chemisorbed Zn^{2+} on Pt, so that expectant Pt_3Zn_{10} intermetallic phase could not be obtained. Based on the hydrogen spillover reduction mechanism, as for the sample formed when the ratio of Pt to Zn was 3:10 and post heat-treatment was under 400 ºC, extra zinc atoms accumulated on the surface of the metal particles, forming zinc oxide when exposed in air, and volatilized between 400 ºC and 500 ºC, preventing particles sintering.

Experimental

Catalysts preparation

The carbon-supported Pt-Zn/C nanoparticles with Pt:Zn nominal ratio of 3:1, 1:1 and 3:10 were prepared using an impregnation reduction method.[42] For example, in a typical synthesis of Pt_3Zn/C, 47.8 mg of $H_2PtCl_6{\cdot}6H_2O$ and 4.2 mg of $ZnCl_2$ were dissolved in de-ionized water, and 80 mg of Vulcan XC-72 carbon support were dispersed in the solution. After ultrasonic mixing for 30 min, the suspension was heated under magnetic stirring to allow the solvent to evaporate and form a smooth, thick slurry. The slurry was dried in a vacuum oven at 40 ºC for 12 h. After being ground in an agate mortar, the resulting dark and free-flowing powder was heated in a tube furnace at 300 ºC under flowing H_2 for 2 h. Finally, the powder was cooled to room temperature under N_2. This sample is denoted as Pt_3Zn/C-300. The as-prepared Pt_3Zn/C catalysts were then annealed at 700 ºC under a H_2 atmosphere for 8 h to form ordered structure. The sample obtained at 700 ºC is denoted as Pt_3Zn/C-700. PtZn/C and Pt_3Zn_{10}/C nanoparticles were also prepared in the same way, and are denoted as PtZn/C-300, PtZn/C-700, Pt_3Zn_{10}/C-300, and Pt_3Zn_{10}/C-700, respectively.

Physical characterization

The as-prepared nanoparticles were characterized by powder X-ray diffraction (XRD) using an X' Pert PRO diffractometer, and diffraction patterns were collected at a scanning rate of 4 º min^{-1} and with a step of 0.02°. The composition of the catalysts was determined by X-ray Fluorescence (XRF) using an EAGLE III spectrometer. Thermal gravimetric analysis (TGA) was conducted on a Pyris1 TGA Instrument at a heating rate of 10 ºC min^{-1}. X-ray photoelectron spectroscopy (XPS) spectrum was obtained using an AXIS-ULTRA DLD-600W Instrument. Transmission electron microscopy (TEM) was performed using a Tecnai G2 20 operated at 200 kV.

Electrochemical measurement

All of the electrochemical measurements were performed under room temperature using a CHI 760e Potentiostat/Galvanostat and a three-electrode electrochemical cell. The working electrode used a glassy carbon disk with 5 mm in diameter. 5 mg of samples were dispersed in 1 mL isopropanol/Nafion hybrid solutions via ultrasonic dispersion to form a homogeneous ink. 5 uL of ink was dropped onto the glassy carbon electrode, and dried naturally. The metal loading of the catalysts on the electrode is about 25 ug cm^{-2}. A Pt wire was used as the counter electrode, and a reversible hydrogen electrode (RHE) was used as the reference electrode. The electrocatalytic activities of different catalysts for HCOOH oxidation were studied in 0.5 M HCOOH containing 0.5 M H_2SO_4 and by cyclic voltammetry (CV), linear sweep voltammetry (LSV), chronoamperometry (CA). CVs were performed between +0.05 and +1.2 V at a scan rate of 50 mV s^{-1}, and LSV was performed between +0.05 and +0.7 V at a scan rate of 1 mV s^{-1}, and CA was performed at a constant potential of +0.4 V for 10 ks. For CO stripping voltammetry, the electrode potential was held at +0.1 V in CO-saturated 0.5 M H_2SO_4 solution for 15 min. N_2 was bubbled into the solution for 15 min to remove the excess CO

dissolved in solution by holding the potential at +0.1 V. Finally, the CO stripping voltammetry was measured in the potential ranging from +0.6 V to +1.1 V at a scan rate of 20 mV s^{-1}.

Results and discussion

Figure 1a shows the XRD patterns of Pt_3Zn/C-300 and Pt_3Zn/C-700. The broad peak at around 25º for all samples was attributed to the (002) planes of carbon support. Four typical diffraction peaks appeared at 40.1º, 46.5º, 67.9º and 81.9º for Pt_3Zn/C-300 (FCC, a = 0.3916 nm), corresponding to (111), (200), (220) and (311) planes. It is noted that the peaks' position shifted to higher angles relative to pure Pt (FCC, a = 0.3920 nm,), of which the corresponding peaks are located at 39.8º, 46.2º, 67.5º and 81.3º (see Figure S1 in the Supporting Information), indicating that the smaller atomic radius Zn has been successfully incorporated into the Pt FCC structure, forming a Pt alloy phase with a shrunk lattice. Except for above mentioned planes, (100), (110), (210), (211), (300), and (310) planes were detected for Pt_3Zn/C-700 (FCC, a = 0.3893 nm), suggesting an ordered Pt_3Zn intermetallic phase (PDF card #03-065-3257) formed. The PtZn intermetallic phase could be obtained at lower temperature. As can be seen in Figure 1a, when reduced in a H_2 atmosphere at 300 ºC, two phases corresponding to the disordered alloy phase and PtZn intermetallic phase appeared for the precursor with Pt:Zn ratio of 1:1. When the temperature was lowered to 200 ºC, only disordered alloy phase was obtained (Figure S3). Interestingly, when the nominal ratio of Pt:Zn was increased to 3:10, there was no phase of intermetallic Pt_3Zn_{10}, while only PtZn intermetallic phase appeared. Moreover, not all precursors were reduced in the H_2 atmosphere at 300 ºC. It can be clearly seen that a diffraction peak appeared at around 15º for the Pt_3Zn_{10}/C-300, which was attributed to the un-reduced $ZnCl_2$ precursor (Figure 1b). Zinc oxide diffraction peaks appeared in the XRD patterns of the Pt_3Zn_{10}/C-400 sample, indicating that zinc atoms could easily move and coat on the surface of the metal particles, and convert to zinc oxides when the sample was exposed to air. The extra zinc atoms volatilized when the annealing temperature was higher than 500 ºC. That is why there was no Pt_3Zn_{10} intermetallic phase to be obtained. As shown in Figure 1b, for the XRD patterns of Pt_3Zn_{10}/C-700, the diffraction peaks at 25.4º, 31.1º, 40.8º, 44.8º, 52.2º, 62.2º, 65.5º, 71.3º, 74.3º and 80.1º correspond to (001), (110), (111), (200), (002), (112), (220), (202), (310) and (311) planes (BCT, a = b = 0.4025 nm, c = 0.3491 nm, PDF card #00-006-0604), indicating that the ordered PtZn intermetallic phase has been successfully obtained.

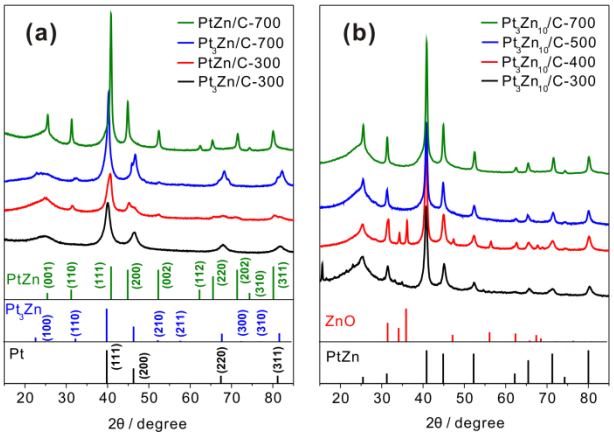

Figure 1. XRD patterns of (a) Pt_3Zn/C and PtZn/C prepared at 300 ºC and after 700 ºC heat-treatment, (b) Pt_3Zn_{10}/C prepared at 300 ºC and after 400, 500 and 700 ºC heat-treatment. Below are the peak positions of standard (a) pure metallic Pt, intermetallic Pt_3Zn and PtZn, and (b) metallic oxide ZnO.

The bulk chemical analysis of the samples was conducted using X-ray fluorescence (XRF). As shown in Figure 2, the actual atomic ratios of Pt:Zn were not in accordance with the nominal ratios because of the Zn volatilization, especially for the samples obtained at high temperature. For example, the atomic ratio of Zn:Pt was 75:25 for Pt_3Zn_{10}/C-300, which was close to the nominal ratio of 10:3. The value decreased with increasing annealing temperature, and reached about 1:1 at 700 ºC, in agreement with the XRD result in Figure 1b that only PtZn intermetallic phase appeared. The actual metal loading was calculated to be 25 wt % for Pt_3Zn/C-300, 26 wt % for Pt_3Zn/C-700, 25 wt % for PtZn/C-300, 28 wt % for PtZn/C-700, and 18 wt % for Pt_3Zn_{10}/C-700, by

using thermal gravimetric analysis (TGA) through the weight loss of carbon support (Figure S4). Compared to nominal metal loading for 20 wt % of all as-prepared samples, the actual metal loading slightly increased because carbon support lost in the synthesis process and the oxide formed when they are exposed to the air. However, the actual metal loading of Pt_3Zn_{10}/C-700 decreased owing to the evaporation of a mass of Zn element.

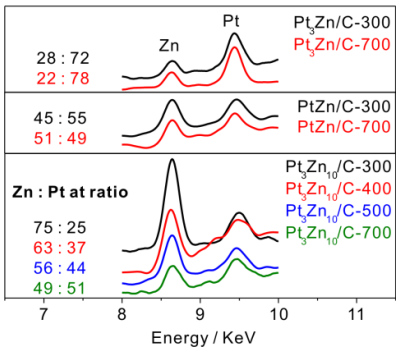

Figure 2. XRF patterns of Pt_3Zn/C and PtZn/C prepared at 300 °C and after 700 °C heat-treatment, and Pt_3Zn_{10}/C prepared at 300 °C and after 400, 500 and 700 °C heat-treatment.

The overview of the TEM images in Figures 3a and b clearly shows that most of the particles dispersed evenly on the carbon support. The particle size distribution, calculated from more than 300 nanoparticles, shows that the mean particle sizes were about 5 nm and 3 nm in diameter (the insets of Figures 3a, b) for Pt_3Zn/C-700 and Pt_3Zn_{10}/C-700, respectively. Zn served as a coating layer, preventing the nanoparticles sintering during high temperature treatment, similar to the previous report about coating PtFe nanoparticles with a layer of MgO.[31] The interplanar spacings are 3.51, 2.87 and 2.21 Å measured from HRTEM micrographs of an individual particle (Figure 3c, d, e), corresponding to {001}, {110} and {111} planes, respectively. The HRTEM image in Figure 3f, which is consistent with the XRD pattern in Figure 1b, clearly shows the PtZn intermetallic phase for Pt_3Zn_{10}/C-700 sample.

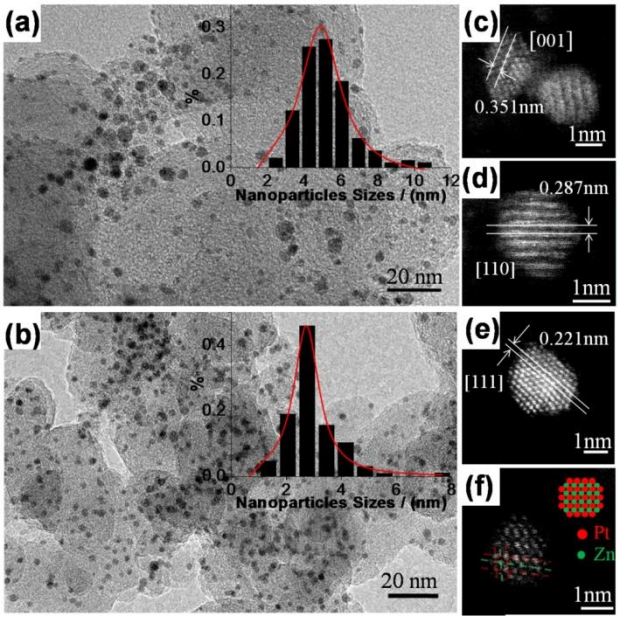

Figure 3. TEM micrographs of Pt_3Zn/C-700 (a) and Pt_3Zn_{10}/C-700 (b), the insets are the corresponding histograms of the particle size distribution and HRTEM micrographs of an individual particle for Pt_3Zn_{10}/C-700 (c, d, e, f).

Table 1. ECSA, onset potentials, mass activities, and specific activities of Pt/C and Pt-Zn/C series catalysts.

samples	ECSA (m^2 g^{-1})	onset potentials (vs. RHE)	mass activities (mA mg^{-1}_{Pt})		specific activities (A m^{-2}_{Pt})	
			0.3 V	0.5 V	0.3 V	0.5 V
Pt/C	75	0.15 V	19.3	115	0.26	1.5
Pt_3Zn/C-300	76	0.12 V	38.2	265	0.50	3.5
PtZn/C-300	64	0.09V	36.2	249	0.57	3.9
Pt_3Zn/C-700	71	0.15 V	27.6	211	0.39	3.0
PtZn/C-700	54	0.15V	22.2	231	0.41	4.3
Pt_3Zn_{10}/C-700	56	0.12 V	39.4	332	0.70	5.9

Figure 4a and Figure S5 compared the CVs of Pt/C and Pt-Zn/C series catalysts in 0.5 M H_2SO_4. It can be seen that there was no well-defined adsorption/desorption peaks on Pt-Zn/C series catalysts, and the hydrogen regions were depressed by the incorporation of Zn into the Pt lattice. Hydrogen adsorption/desorption behaviors also varied with different phases and the content of Zn. The electrocatalytic activities for formic acid oxidation on different catalysts were evaluated by steady state linear sweep voltammograms (LSV) (Figure 4b and Figure S6). All the currents were normalized to the mass of Pt on the electrodes. The electrochemical testing results are summarized in Table 1. It can be seen that the onset potential for HCOOH electrooxidation on Pt-Zn/C series catalysts was 30 mV more negative than that on Pt/C except for the samples Pt_3Zn and PtZn after post-treatment at 700 ºC. The oxidation currents on Pt_3Zn and PtZn were higher than those samples after post-treatment at 700 ºC. However, structurally ordered intermetallic nanocatalysts Pt_3Zn and PtZn after post-treatment at 700 ºC are more durable than chemically disordered solid solution Pt_3Zn/C-300 alloy and mixed phase PtZn/C-300 (Figure 4d). As for the oxidation current at a given potential of +0.5 V, the mass activities of the Pt-Zn/C series catalysts were 2~3 times higher than that of Pt/C (Figure 4c). Moreover, the current densities on Pt_3Zn_{10}/C-700 and Pt_3Zn/C-700 electrodes are 332 and 211 mA mg^{-1}_{Pt}, which are ~2.9 and ~1.8 times higher than that on Pt/C electrode at +0.5 V. Obviously, Pt_3Zn_{10}/C-700 exhibited the highest activity and durability among Pt-Zn/C series catalysts.

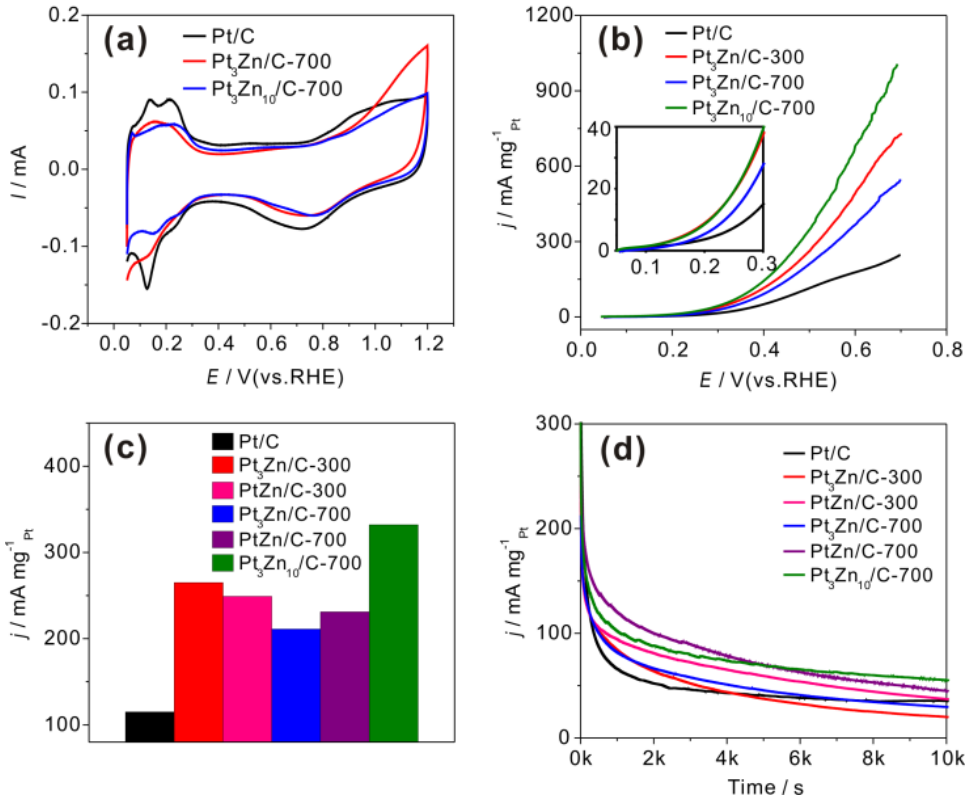

Figure 4. Electrochemical test results of Pt-Zn/C and Pt/C catalysts. (a) Cyclic voltammograms in 0.5 M H_2SO_4 purged with N_2 at room temperature and a sweep rate of 20 mV s^{-1}. (b) Linear sweep voltammograms in 0.5 M H_2SO_4 + 0.5 M HCOOH at sweep rate of 1 mV s^{-1}. (c) Comparison of mass activities at +0.5 V. (d) Current vs. time plots measured by chronoamperometry at +0.4 V.

The specific surface activities of the catalysts were evaluated by normalizing current to electrochemically active specific surface area (ECSA), which was determined by CO stripping method. As shown in Figure 5a, the ECSAs were calculated from the CO oxidation charge after subtracting the background current, which were presented in Table 1. It can be seen from Figure 5a that all the Pt-Zn/C series catalysts exhibited more negative onset potential for CO oxidation than that on Pt/C, indicating a weaker oxophilicity of Pt centers in Pt-Zn catalysts, which could facilitate the removal of CO poisoning during the HCOOH oxidation process. Moreover, onset potential for CO oxidation on PtZn phase was more negative than that on Pt_3Zn phase, and there are two peaks on PtZn/C-300, which was consistent with XRD pattern in Figure 1a, clearly showed PtZn/C-300 was the mixed phase. Figure 5b and Figure S7 showed the CVs of different catalysts. The anodic currents in the forward scan on Pt-Zn series catalysts were observably larger than that on Pt, indicating that the as-prepared catalysts are less susceptible to CO poisoning. Figure S8 shows the CVs in HCOOH solution after different electrochemical treatment conditions. By increasing the potential, two current peaks in the forward scan became more obvious, which was similar to the characteristic on Pt/C, due to rapid dissolution of Zn on the surface of the electrode at high potential. Zn played an important role to catalyze formic acid oxidation due to the ligand effect, reducing the number of Pt ensemble that is required to form adsorbed CO, and thus inhibiting HCOOH decomposition to form adsorbed CO.[22] To avoid size effect, specific activities were used to evaluate the catalytic performance. As-prepared Pt-Zn series catalysts exhibited higher specific surface activities at +0.5 V than Pt/C (Figure 5c). Pt_3Zn_{10}/C-700 exhibited the highest activity among the Pt-Zn catalysts, which is ~3 times and ~2 times higher than that on Pt/C and Pt_3Zn/C-700 catalysts, respectively. In contrast to the comparison of mass activities, the specific activity of more orderly PtZn/C-700 is higher than PtZn/C-300 with the mixed phase. However, the specific activity of Pt_3Zn/C-700 is still lower than Pt_3Zn/C-300 as before, probably due to the ligand effect of Pt_3Zn/C-700 was weakened because the surface Zn volatilized during high-temperature treatment and the surface content of Zn was reduced, as detected by XPS measurement (see Figure S9 in the Supporting Information) that the surface ratio of Pt:Zn was 72:28 and 79:21 for Pt_3Zn/C-300 and Pt_3Zn/C-700, respectively. As shown in Figure 5d and Figure S10, XPS analysis could

explain the relationship between structure and activity. The observed positive shifts in the Pt 4f and Zn 2p indicated that Pt-Zn binding energy became stronger. It has been reported that stronger binding energy results in the increased surface energy, and metal NPs with high-energy surfaces exhibit high catalytic performance.[43] Here, the sort of the binding energy is consistent with the one of the activity.

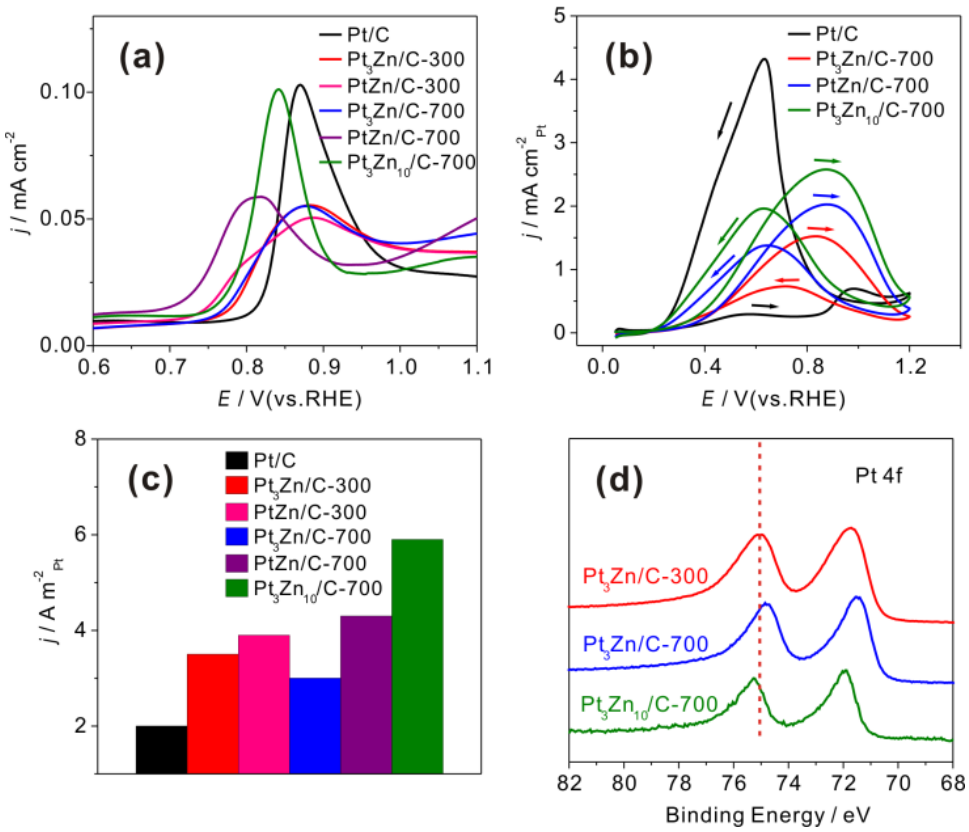

Figure 5. (a) CO stripping voltammograms on different electrodes in 0.5 M H_2SO_4 at a sweep rate of 20 mV s^{-1}. (b) Cyclic voltammograms of the Pt/C, Pt_3Zn/C-700, PtZn/C-700 and Pt_3Zn_{10}/C-700 in 0.5 M H_2SO_4 + 0.5 M HCOOH at a sweep rate of 50 mV s^{-1}. (c) Comparison of specific activities at +0.5 V on different electrodes. (d) XPS fine spectra of Pt 4f of Pt_3Zn/C-300, Pt_3Zn/C-700 and Pt_3Zn_{10}/C-700.

Conclusions

In summary, structurally ordered Pt_3Zn and PtZn intermetallic nanoparticles have been successfully synthesized via an impregnation reduction method followed by post heat-treatment. The obtained nanoparticles were highly dispersed on the carbon support with small mean particle sizes of 3 to 5 nm, owing to evaporation of the zinc element, preventing the particles sintering at high temperature. For Pt_3Zn/C catalysts, the sample after 700 °C heat-treatment exhibited lower activity than before heat-treatment, which was credited to the ligand effect that surface Zn volatilized during high-temperature treatment and the surface content of Zn was reduced. However, Pt_3Zn/C-700 is more durable than Pt_3Zn/C-300 because of its chemically ordered structure. Among the Pt-Zn/C series catalysts, the nanoparticles with PtZn intermetallic phase exhibited better performance than those with Pt_3Zn intermetallic phase, and Pt_3Zn_{10}/C-700 nanoparticles with PtZn intermetallic phase show the best activity and stability for formic acid electrooxidation. As depicted by cyclic voltammetry and CO-stripping analysis, alloying with the Zn element significantly enhances the tolerance to CO poisoning, compared to Pt/C, which makes an enormous contribution to the catalytic performance at anode. Currently, the price of Zn is low, and the synthesis procedure is facile and amenable to scale up, making Pt-Zn/C series nanoparticles are promising as catalysts for direct formic acid fuel cells.

Acknowledgements

This work was supported by the National Natural Science Foundation (21306060), the Program for New Century Excellent Talents in Universities of China (NCET-13-0237), the Doctoral Fund of Ministry of Education of China (20130142120039), the Fundamental Research Funds for the Central University (2013TS136, 2014YQ009). We thank Analytical and Testing Center of Huazhong University of Science& Technology for allowing us to use its facilities. S/TEM work was carried out at the Center for Functional Nanomaterials, Brookhaven National Laboratory, which is supported by the U.S. Department of Energy, Office of Basic Energy Sciences, under Contract No.DE-SC0012704.

Notes and references

[a] Key Laboratory for Large-Format Battery Materials and System, Ministry of Education, Hubei Key Laboratory of Material Chemistry and Service Failure, School of Chemistry and Chemical Engineering, Huazhong University of Science & Technology, Wuhan, 430074, P.R. China. E-mail: wangdl81125@hust.edu.cn.

[b] Center for Functional Nanomaterials, Brookhaven National Laboratory, Upton, NY, USA.

[c] Department of Materials Science and Engineering SUNY Stony Brook University, Stony Brook, NY, 11794, USA.

Electronic Supplementary Information (ESI) available: [details of any supplementary information available should be included here]. See DOI: 10.1039/b000000x/

1 X. Wang, J. M. Hu and I. Hsing, *J. Electroanal. Chem.*, 2004, **562**, 73.

2 Y. W. Rhee, S. Y. Ha and R. I. Masel, *J. Power Sources*, 2003, **117**, 35.

3 K. J. Jeong, C. M. Miesse, J. H. Choi, J. Lee, J. Han, S. P. Yoon, S. W. Nam, T. H. Lim and T. G. Lee, *J. Power Sources*, 2007, **168**, 119.

4 C. Venkateswara Rao, C. R. Cabrera and Y. Ishikawa, *J. Phys. Chem. C*, 2011, **115**, 21963.

5 X. Zhao, M. Yin, L. Ma, L. Liang, C. Liu, J. Liao, T. Lu and W. Xing, *Energy Environ. Sci.*, 2011, **4**, 2736.

6 X. Yu and P. G. Pickup, *J. Power Sources*, 2008, **182**, 124.

7 J. Lović, A. Tripković, S. L. Gojković, K. D. Popović, D. Tripković, P. Olszewski and A. Kowal, *J. Electroanal. Chem.*, 2005, **581**, 294.

8 A. Cuesta, G. Cabello, M. Osawa and C. Gutiérrez, *ACS Catal.*, 2012, **2**, 728.

9 S. Park, Y. Xie and M. J. Weaver, *Langmuir*, 2002, **18**, 5792.

10 A. V. Tripković, K. Đ. Popović and J. D. Lović, *J. Serb. Chem. Soc.*, 2003, **68**, 849.

11 E. Casado-Rivera, D. J. Volpe, L. Alden, C. Lind, C. Downie, T. Vázquez-Alvarez, A. C. Angelo, F. J. DiSalvo and H. D. Abruna, *J. Am. Chem. Soc.*, 2004, **126**, 4043.

12 S. Kang, J. Lee, J. K. Lee, S. Y. Chung and Y. Tak, *J. Phys. Chem. B*, , 2006, **110**, 7270.

13 X. Yu and P. G. Pickup, *Electrochim. Acta*, 2011, **56**, 4037.

14 T. Schmidt, R. Behm, B. Grgur, N. Markovic and P. Ross, *Langmuir*, 2000, **16**, 8159.

15 M. Arenz, V. Stamenkovic, T. J. Schmidt, K. Wandelt, P. N. Ross and N. M. Markovic, *Phys. Chem. Chem. Phys.*, 2003, **5**, 4242.

16 B. Liu, H. Li, L. Die, X. Zhang, Z. Fan and J. Chen, *J. Power Sources*, 2009, **186**, 62.

17 N. V. Long, T. D. Hien, T. Asaka, M. Ohtaki and M. Nogami, *Int. J. Hydrogen Energy*, 2011, **36**, 8478.

18 Y. X. Wang and T. H. Chen, *Chinese Chem. Lett.*, 2014, **25**, 907.

19 Y. Kim, H. J. Kim, Y. S. Kim, S. M. Choi, M. H. Seo and W. B. Kim, *J. Phys. Chem. C*, 2012, **116**, 18093.

20 J. H. Choi, K. J. Jeong, Y. Dong, J. Han, T. H. Lim, J. S. Lee and Y. E. Sung, *J. Power Sources*, 2006, **163**, 71.

21 Q. He, B. Shyam, M. Nishijima, X. Yang, B. Koel, F. Ernst, D. Ramaker and S. Mukerjee, *J. Phys. Chem. C*, 2013, **117**, 1457.

22 A. Miura, H. Wang, B. M. Leonard, H. D. Abruna and F. J. DiSalvo, *Chem. Mater.*, 2009, **21**, 2661.

23 Y. Kang, J. B. Pyo, X. Ye, T. R. Gordon and C. B. Murray, *ACS Nano*, 2012, **6**, 5642.

24 C. T. Hsieh, W. M. Hung, W. Y. Chen and J. Y. Lin, *Int. J. Hydrogen Energy*, 2011, **36**, 2765.

25 Q. Chen, J. Zhang, Y. Jia, Z. Jiang, Z. Xie and L. Zheng, *Nanoscale*, 2014, **6**, 7019.

26 G. A. El-Nagar and A. M. Mohammad, *Int. J. Hydrogen Energy*, 2014, **39**, 11955.

27 D. Wang, H. L. Xin, R. Hovden, H. Wang, Y. Yu, D. A. Muller, F. J. DiSalvo and H. D. Abruña, *Nat. Mater.*, 2013, **12**, 81.

28 D. Wang, Y. Yu, H. L. Xin, R. Hovden, P. Ercius, J. A. Mundy, H. Chen, J. H. Richard, D. A. Muller and F. J. DiSalvo, *Nano Lett.*, 2012, **12**, 5230.

29 S. Zhang, S. Guo, H. Zhu, D. Su and S. Sun, *J. Am. Chem. Soc.*, 2012, **134**, 5060.

30 Q. Li, L. Wu, G. Wu, D. Su, H. Lv, S. Zhang, W. Zhu, A. Casimir, H. Zhu and A. Mendoza-Garcia, *Nano Lett.*, 2015, **15**, 2468.

31 J. Kim, Y. Lee and S. Sun, *J. Am. Chem. Soc.*, 2010, **132**, 4996.

32 S. Zhang, X. Zhang, G. Jiang, H. Zhu, S. Guo, D. Su, G. Lu and S. Sun, *J. Am. Chem. Soc.*, 2014, **136**, 7734.

33 H. Chen, D. Wang, Y. Yu, K. A. Newton, D. A. Muller, H. C. Abruña and F. J. DiSalvo, *J. Am. Chem. Soc.*, 2012, **134**, 18453.

34 S. Prabhudev, M. Bugnet, C. Bock and G. A. Botton, *ACS Nano*, 2013, **7**, 6103.

35 X. Ji, K. T. Lee, R. Holden, L. Zhang, J. Zhang, G. A. Botton, M. Couillard and L. F. Nazar, *Nat. Chem.*, 2010, **2**, 286.

36 K. Mayrhofer, B. Blizanac, M. Arenz, V. Stamenkovic, P. Ross and N. Markovic, *J. Phys. Chem. B*, 2005, **109**, 14433.

37 M. Arenz, K. J. Mayrhofer, V. Stamenkovic, B. B. Blizanac, T. Tomoyuki, P. N. Ross and N. M. Markovic, *J. Am. Chem. Soc.*, 2005, **127**, 6819.

38 M. Shao, A. Peles and K. Shoemaker, *Nano Lett.*, 2011, **11**, 3714.

39 Z. Cui, H. Chen, M. Zhao, D. Marshall, Y. Yu, H. Abruña and F. J. DiSalvo, *J. Am. Chem. Soc.*, 2014, **136**, 10206.

40 B. M. Leonard, Q. Zhou, D. Wu and F. J. DiSalvo, *Chem. Mater.*, 2011, **23**, 1136.

41 J. Wang, Y. Wang, S. Xie, M. Qiao, H. Li and K. Fan, *Appl. Catal. A*, 2004, **272**, 29.

42 D. Wang, H. L. Xin, H. Wang, Y. Yu, E. Rus, D. A. Muller, F. J. DiSalvo and H. D. Abruña, *Chem. Mater.*, 2012, **24**, 2274.

43 G. V. Ramesh, R. Kodiyath, T. Tanabe, M. Manikandan, T. Fujita, N. Umezawa, S. Ueda, S. Ishihara, K. Ariga and H. Abe, *ACS Appl. Mater. Interfaces*, 2014, **6**, 16124.